Journal of Applied Fluid Mechanics, Vol. 18, No. 10, pp. 2550-2567, 2025.
Available online at www.jafmonline.net, ISSN 1735-3572, EISSN 1735-3645.
https://doi.org/10.47176/jafm.18.10.3216

Analysis of Flow Resistance in Trifurcation Fluid Networks

M. Mustafaoglu †, M. Kaan Yesilyurt, İ. Kotcioglu and M. Allahyari

Atatürk University, Engineering Faculty, 25240, Erzurum, Turkey

†*Corresponding Author Email: mansour@atauni.edu.tr*

ABSTRACT

In branch-like structures, branching parameters such as branching diameter, angle, length and number of levels, as well as branching number, have been important research topics in the field of fluid transport. In such flow systems, the fluid is transported to different branches with the help of the main pipe. The present study aims to investigate equi-diameter and unequi-diameter trifurcation flow systems designed according to Murray's law on flow resistance and pressure loss for a given velocity and pressure. By examining the flow model passing through the trifurcation flow system with 3D flow modeling, designs have been developed to provide the lowest pressure, least vortex formation and most efficient flow. The flow resistance for trifurcation branching for equal-diameter and unequal-diameter branching networks and terminal branch diameters are compared, and the lowest energy loss was found to occur when the diameter of two branches is equal at all three branches.

Article History

Received November 9, 2024
Revised May 6, 2025
Accepted May 20, 2025
Available online August 5, 2025

Keywords:

Trifurcation
Branching
Fluid Network
Flow resistance
Computational fluid dynamics

1. INTRODUCTION

The study of fluidic networks covers a wide range of disciplines, including physics, biology, and materials science. The furcation flow systems, which can be considered a specific type of behavior occurring within fluidic networks, have prominent importance in both natural and engineered systems. Furcation flow systems are integral to several biological processes such as nutrient transport, waste removal, and signal transmission. The structural design of fluidic networks can significantly influence their performance (Beighley et al., 2012) and the branching structure in furcation flow systems minimizes energy loss. This biomimetic branching network structure has received interest in industrial processes for their efficiency.

Fluidic network designs should accommodate varying fluid properties while effectively balancing flow rates and pressure drops. Such designs, therefore, need optimization of several parameters such as flow efficiency, energy loss and geometric configurations. Murray defined a theoretical framework (Murray, 1926a, b, 1927) to reduce power consumption. It puts that the optimal configuration of furcating tubes minimizes energy dissipation by balancing the radii of parent and daughter tubes (Smink et al., 2023). Murray's Law has been extensively applied to biological and engineering systems for optimizing fluid transport (Zimmerman & Tartakovsky, 2020; Smink et al., 2023). Maximizing flow efficiency is the second critical principle in fluid network optimization. This involves ensuring that fluid transport occurs with minimal resistance and maximal throughput. Geometric configuration is of prominent importance in terms of flow efficiency.

The applicability of furcation flow networks engineering systems has been remarkable for researchers. The furcation number and furcation angles of the branches conform to a certain growth law. Generally, furcation flow systems such as bifurcation and trifurcation systems consist of a three-dimensional volume on a two-dimensional surface that carries the fluid inside. These geometries are symmetrical and unsymmetrical shapes made up of smaller parts that are similar in nature. Mathematical definitions suitable for the physics of such geometries are being developed. Bifurcation and trifurcation networks, such as those involving trees, leaves, blood vessels, and nervous and respiratory systems, are also common in nature.

Significant advancements were recorded in the study of fluidic networks. But much of the existing literature has predominantly focused on bifurcation systems (Bejan, 1997; Bejan & Errera, 1997; Bejan 2000, Bejan 2001; Chen & Cheng, 2002; Calamas & Baker, 2013; Luo et al., 2018; Xu & Yu, 2006; Yu et al., 2012) due to their prevalence in both natural and engineered systems. For instance, the dynamics of red blood cell (RBC) partitioning at bifurcations were extensively studied (Balogh & Bagchi, 2018; Ye & Li-na, 2019; Ostalowski & Tan, 2022). Other studies focused on the investigation

NOMENCLATURE

l_{n-1}	length of (n - 1)th fork	$R_{n-t,total}$	total flow resistance from Nth to (N - t) th
l_n	length of nth fork	R_0	flow resistance of first fork
l'_n	length of n'th fork	r	radii of first fork in ED network
l''_n	length of n"th fork	r_0	radii of first fork in UD network
R_{n-1}	flow resistances of (n- 1)th fork	r_{n-1}	radius of (n - 1) th fork
R_n	flow resistances of nth fork	r_n	radius of nth fork
R'_n	flow resistances of n'th fork	r'_n	radius of n"th fork
R''_n	flow resistances of n"th fork	r''_n	radius of n"th fork
R_{total}	total flow resistances in network		

of path selection of spheres and the Zweifach–Fung effect, which describes the preferential flow of particles in bifurcating channels (Doyeux et al., 2011; Wang et al., 2018).

On the other hand, few research has focused on trifurcation networks while they have good potential applications in various fields such as biomedical engineering, microfluidics, and energy systems. This limited interest could be attributed to the increased complexity associated with three-way branching as their analysis is much more complicated due to additional variables and interactions. Guha and Pradhan (2017) studied secondary flows in three-dimensional branching networks and reported that mass distribution became more complex in trifurcation setups (Guha & Pradhan, 2017; Pradhan & Guha, 2019). But research in this field is limited. A brief of research on trifurcation networks is presented in Table 1.

The flow behavior in trifurcation systems is an important aspect to study in order to improve the efficiency of fluidic devices. Additionally, research on trifurcation systems can help us understand complex biological systems, such as the human circulatory system (Menon, 2024; Ostalowski & Tan, 2022). Trifurcations also provide greater flexibility in design of multi-branch fluid distribution systems. Trifurcation flow systems also have applications across various engineering domains, being particularly effective in complex or energy-efficient cooling systems with varying geometries and pressures.

In biomedical engineering, trifurcation networks play a crucial role in blood circulation, particularly in arterial and venous branching where efficient fluid transport is vital for physiological function (Menon, 2024). Understanding flow resistance and pressure distribution in these networks can help better understand cardiovascular diseases, where alterations in vessel furcation geometry contribute to abnormal hemodynamics (Ostalowski & Tan, 2022).

Furthermore, trifurcation networks are extensively utilized in microfluidics and lab-on-a-chip technologies, where efficient splitting and transport of fluids are essential for chemical and biological assays (Kim & Peskin, 2008). In industrial applications, trifurcation-based cooling networks are employed in thermal management of electronics and heat exchanger designs, where optimal branching structures minimize energy dissipation and enhance heat transfer efficiency (Smink et al., 2023).

Studies on trifurcation networks, summarized in Table 1, primarily focus on different aspects of flow behavior, energy dissipation, and structural optimization. Experimental studies, such as that of Kawano and Fuchiwaki (2022), have investigated pressure drops in trifurcated cooling systems, emphasizing turbulent kinetic energy losses due to flow separation. Theoretical and numerical analyses, including Smink et al. (2023), have examined optimal branching angles to minimize energy dissipation in fluidic networks. Other studies, such as those by Kim and Peskin (2008), have explored density variation effects on pressure drop in incompressible fluid networks, while Guha and Sengupta (2016) analyzed convection effects in branching structures. While the studies cited duly highlight the complexity of trifurcation networks, they do not comprehensively address the relationship between branching angles, diameter variations, and flow resistance in a unified framework.

In this regard, we present in this study an analytical and numerical analysis of trifurcation networks by extending well-established application of Murray's law in bifurcation networks (Zimmerman & Tartakovsky, 2020; Smink et al., 2023) into trifurcation systems where its direct applicability remains understudied.

In fact, when directly applied to trifurcation networks, several limitations arise regarding the implementation of Murray's Law. First, Murray's Law assumes Newtonian fluid behavior, whereas many biological and industrial fluids exhibit non-Newtonian properties (e.g., blood, polymer solutions) that introduce additional shear stress variations that are not captured by classical Murray's Law formulations (Guha & Pradhan, 2017).

Second, the law assumes steady, laminar flow conditions, but in real-world systems, flow instabilities, turbulence, and secondary vortices may arise at trifurcation junctions, especially at higher Reynolds numbers (Zhao et al., 2020). Experimental studies on branching networks have reported localized turbulence effects that contribute to increased pressure losses, deviating from the predictions of Murray's Law (Wang et al., 2018). Finally, the geometric idealizations in Murray's Law (e.g., uniform furcation angles, symmetrical branching) may not hold in natural or engineered trifurcation systems, where asymmetry and variability significantly impact flow characteristics.

To address these limitations and allow for a more realistic evaluation of flow resistance, velocity distributions, and energy dissipation under diverse conditions, this study was configured to integrate analytical

Table 1 Details of studies on trifurcation flow networks over the last decade

Ref	Type of Study	Properties of Trifurcation Network Studied	Important Parameters	Remarks
Kawano and Fuchiwaki (2022)	Experimental	Pressure drop in cooling systems	Turbulent kinetic energy	Identified pressure drops due to turbulent kinetic energy in trifurcation setups, emphasizing the role of flow separation.
Smink et al. (2023)	Theoretical Numerical	Branched fluidic network	Furcation angle	Investigated optimal angles for trifurcations to minimize energy dissipation. They established a relationship between geometry and flow efficiency.
Kim and Peskin (2008)	Numerical	Fluid network for Incompressible fluid with non-uniform density	Density variation, branch diameters	Effect of varying branch diameters on flow patterns in incompressible fluid dynamics were analyzed; Non-uniform density was reported to induce variations in pressure drop.
Guha and Sengupta (2016)	Numerical	Natural convection above horizontal plates	Aspect ratio, flow conditions	Geometric features were assessed. Aspect ratio was found to be influential on pressure drop and flow uniformity across branches.
Yu et al. (2012)	Experimental & Numerical	Microchannel heat and fluid transfer	Branch length, fractal scaling, channel size	Pressure drop increased in larger scale networks but minimized at micro-scales.
Calamas and Baker (2013)	Numerical (CFD)	Thermal systems for natural convection	Heat transfer coefficient, thermal conductivity	Increased complexity increased pressure drop but improved heat dissipation.

and numerical approaches to bridge the gap between theoretical predictions and practical applications.

As a result, we aimed to compensate the analytical simplicity and limitations of Murray's Law with Computational Fluid Dynamics (CFD) methods that offer a modern and versatile tool for analyzing fluid flow in complex geometries like trifurcations. CFD also enables detailed simulation of fluid behavior under diverse conditions by solving the Navier-Stokes equations to account for factors like turbulence, non-Newtonian fluids, and complex geometries (Jia, 2020; Chen, 2024).

Using CFD is particularly valuable in trifurcation networks because the fluid dynamics are considerably more complex than in bifurcations. This complexity is due to the additional branching pathways and the resulting variations in flow resistance, shear stress, and velocity distributions.

The combination of Murray's Law with CFD analysis is powerful in exploring deviations from the idealized conditions. This combination allows modeling of the effects of different branch configurations. Flow complexities induced by angle variations, diameter changes, which cannot be captured by Murray's Law alone (Smink et al., 2023; Chen, 2024) can be observed with CFD analysis. In engineered fluid transport systems, integrating Murray's Law with CFD can lead to the design of optimal geometries that balance energy efficiency and flow distribution.

In this regard, the present study is intentionally confined to Newtonian fluid assumptions in order to maintain consistency with Murray's Law and to enable a sound comparison between analytical and numerical results. This choice further allows the study to isolate the influence of geometrical features and branching structure without the added rheological complexities such as shear-thinning behavior and viscoelasticity.

2. MATERIALS AND METHODS

The study of furcation fluidic networks employs both analytical and numerical methods, which utilize various mathematical and computational tools. CFD, one of the most commonly used techniques, play a crucial role in the analysis of furcation fluidic networks. It provides a numerical approach to solving the governing equations of fluid motion and allows for the simulation of complex flow patterns in various geometries.

The present study involves analytical and numerical analyses of two two-level trifurcation systems: an equi-diameter (ED) network and an unequi-diameter (UD) network, presented in detail in Fig. 1.

2.1. Analytical Method

To establish a theoretical foundation for analyzing trifurcation flow networks, we apply Murray's Law, which minimizes energy expenditure by balancing the radii of branching tubes (Murray, 1926a, b).

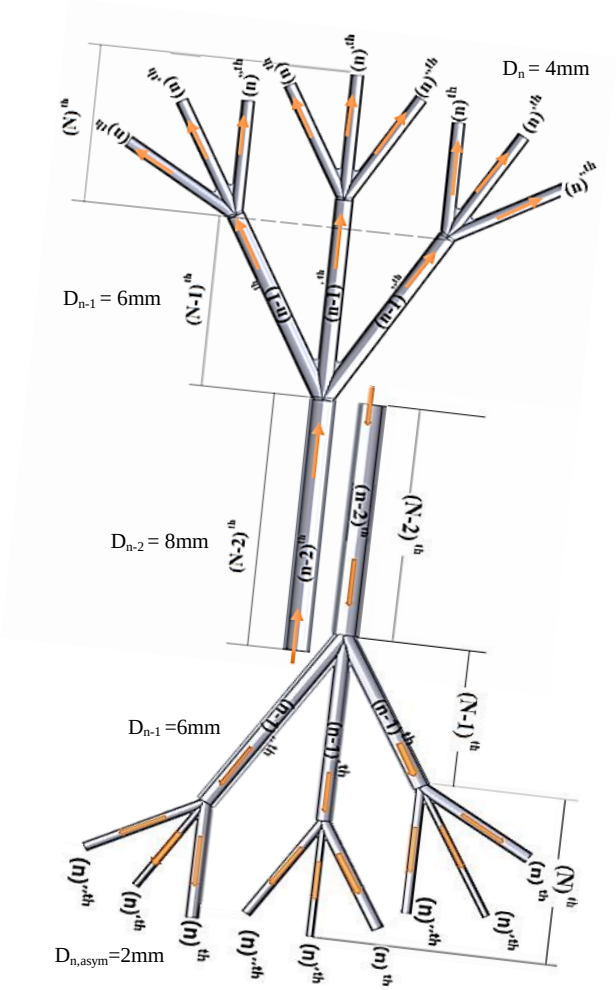

Fig. 1 Schematic diagram of the two-level ED (upper) and UD (lower) trifurcation flow system

2.1.1. Murray's Law

The modern approach to the physical furcation modeling is rooted from the exploration that transport systems in plants and animals tend to furcate after a certain straight into branches to minimize energy expenditures and to facilitate transport. The growth is justified by the compensatory benefits of the resulting structure.

One of the important relationships in the branching network of fluid circulations used is Murray's law (Murray, 1926a, b, 1927). The law was originally formulated in 1926 by Cecil D. Murray to explain the optimal design of a circulatory system and it provides a theoretical framework for furcation fluid networks. The law posits that for a network of tubes (or vessels) that furcate, the radii of the parent vessel and its daughter vessels are related in a specific way that minimizes the energy required for the transport of fluid within.

The derivation begins with the Hagen-Poiseuille equation, which describes the volumetric flow rate (Q) through a cylindrical vessel as:

$$Q = \frac{\pi r^4 \Delta P}{8\mu l} \tag{1}$$

The relationship that leads to Murray's law is obtained by applying the law of conservation of mass at the bifurcation point and assuming steady, incompressible flow conditions. The optimal configuration for furcation systems occurs when the sum of the cubes of the forks' radii equals the cube of the parent tube radius, is expressed mathematically as follows:

$$r_0^3 = r_1^3 + r_2^3 + \cdots + r_n^3 \tag{2}$$

where r_0 and r_n are the radii of parent and the n branches furcating from the parent, respectively.

Murray's law is instrumental in understanding optimization of fluid flow in furcating networks and has been extended and adapted for use in engineered systems, such as microfluidic devices. Smink et al. (2023) emphasize the importance of applying Murray's theory to design branched fluidic networks that minimize energy dissipation. Adhering to the principles of Murray's law, effective transport of fluids with reduced energy costs can be achieved. A large number of studies have addressed this topic, mainly from a biomedical science perspective, but since they all show poor agreement with experimental data, it is useful to examine this issue in more detail. It is then argued that in real branching networks, the true optimality criteria (i.e., in the evolutionary sense of the "driving force") may be quite different from the assumptions made in the H-M law literature, which explains the poor predictive value of the law. Some model settings that include resource-based cost/benefit of bifurcation are presented and discussed.

Smink et al. (2023) extended Murray's theory to include various fluid rheologies, such as non-Newtonian and yield-stress fluids and introduced a straightforward graphical method to determine optimal radii in furcation networks. They reported that the wall shear stress was uniform over the whole network and that the velocity profile was comparable. They also examined the impact of the non-optimal channel radius on the energy consumption of the network and demonstrated that their method was applicable across a variety of systems.

Murray predicts the diameters or forks in fluid networks such that cost and maintenance is minimized. Such flow systems have a similar sequential structure and they have minimum flow resistances while delivering the flow to the extreme points.

2.1.2. Flow Resistance in Trifurcation Network

In this study, the network structure of equi- and unequi-diameter branches is shown in Fig. 1. This figure shows a single inlet, two-level, three-branch, nine-output flow system. To simplify the relation for the calculation equation, we use λ, β, α, γ, δ1, and δ2 in the forms below:

$$\lambda = \frac{r_n}{r_n''} \qquad \beta = \frac{r_n'}{r_n''} \qquad \alpha = \frac{r_n''}{r_{n-1}}$$

$$\delta_1 = \frac{l_n}{l_n'} \qquad \delta_2 = \frac{l_n'}{l_n''} \qquad \gamma = \frac{l_{n-1}}{l_n}$$

Here, and in the subsequent mathematical expressions, the prime (') and double prime (") notation denote different branch levels in the trifurcation network.

Specifically, (') represents the first daughter branch, while (") denotes the second daughter branch.

In flow systems, minimizing flow resistance and thermal resistance is an important principle in basic engineering practice. Only pressure differences are sufficient to cause flow to occur, and only resistance is sufficient to study the flow characteristics. According to the design of the branches given in Fig. 1, utilizing Murray's law at the *N*-1th and *N*-2th levels in fully developed incompressible laminar flow, the total flow resistances between the daughter and the parent can be expressed by the following equations.

$$R_{n-1,total} = R_{n-1} + \frac{1}{\frac{1}{R_n} + \frac{1}{R_n'} + \frac{1}{R_n''}} \tag{3}$$

and

$$R_{n-2,total} = R_{n-2} + \frac{1}{\frac{1}{R_{n-1,total}} + \frac{1}{R'_{n-1,total}} + \frac{1}{R''_{n-1,total}}} \tag{4}$$

The value of viscous resistance for flow in a single pipe in branched structures is determined by a Poiseuille-type parabolic flow profile for Newtonian fluids. Poiseuille flow is given by Murray's law in the following equation:

$$r_{n-1}^3 = r_n^3 + r_n'^3 + r_n''^3 \tag{5}$$

$$r_{n-2}^3 = r_{n-1}^3 + r_{n-1}'^3 + r_{n-1}''^3 \tag{6}$$

For *n* number branched pipes, the general form of Murray's law can be defined as

$$r_n^3 = \sum_{i=1}^{k} r_{n+1,i}^3 \tag{7}$$

where *n* is the parent branch, *n*+1 is the daughter, and *k* is the branching level number in each furcation. For example, it departs from the first-order branch at the level $k = 1$, $n=3$, and the second-order branch at the level $k = 2$, $n = 9$. At each furcation, there are *n*th, *n'*th and *n''*th branches. To have branches with equal diameters, the β and λ values must be 1 according to the above definitions. If $\beta=1$, then $r_n' = r_n''$, and if $\lambda=1$, then $r_n = r_n''$; thus, $r_n = r_n' = r_n''$, which means that the tree branches are equal. If $\beta=1$ but $\lambda\neq1$ or $\beta\neq1$ but $\lambda=1$, the branch diameter is equal (ED), but other branches are not equal. If $\beta\neq1$ and $\lambda\neq1$, then all three branches have different diameters (UD). The equation given according to the radii in Eq. 6 is further simplified according to the level and the number of branches. The relationships between them in terms of radii and lengths are as defined above. In each step/level of the network with unequal and multiple branches, the α, β, γ, λ, δ_1 and δ_2 parameters can be obtained as follows.

$$\alpha = \frac{1}{\sqrt[3]{1 + \lambda^3 + \beta^3}} \tag{8}$$

$$\frac{r_n}{r_{n-1}} = \frac{r_n}{r_n''} \times \frac{r_n''}{r_{n-1}} = \beta\alpha \tag{9}$$

$$\frac{r_{n-1}}{r_{n-2}} = \frac{r_{n-1}}{r_{n-1}''} \times \frac{r_{n-1}''}{r_{n-2}} = \beta\alpha \tag{10}$$

$$\frac{r_n'}{r_{n-1}} = \frac{r_n'}{r_n''} \times \frac{r_n''}{r_{n-1}} = \lambda \tag{11}$$

$$\frac{r_{n-1}'}{r_{n-2}} = \frac{r_{n-1}'}{r_{n-1}''} \times \frac{r_{n-1}''}{r_{n-2}} = \lambda \tag{12}$$

$$\frac{l_{n-1}}{l_n'} = \frac{\gamma . l_n}{\frac{l_n}{\delta}} = \gamma . \delta_1 \tag{13}$$

$$\frac{l_{n-2}}{l_{n-1}'} = \frac{\gamma . l_{n-1}}{\frac{l_{n-1}}{\delta}} = \gamma . \delta_2 \tag{14}$$

$$\frac{l_{n-1}}{l_n''} = \frac{\gamma . l_n}{\frac{l_n'}{\delta_2}} = \frac{\gamma l_n \delta_2}{\frac{l_n}{\delta_1}} = \gamma . \delta_1 \delta_2 \tag{15}$$

$$\frac{l_{n-2}}{l_{n-1}''} = \frac{\gamma . l_n - 1}{\frac{l_{n-1}'}{\delta_2}} = \frac{\gamma l_{n-1} \delta_2}{\frac{l_{n-1}}{\delta_1}} = \gamma . \delta_1 \delta_2 \tag{16}$$

The flow impedance (*P*/*Q*) of a tube is important information in the design of a flow system (Smink et al., 2023). With the use of the Hagen–Poiseuille equation, the flow resistance and the flow rate in a channel of the k^{th} level are obtained by the following equations:

$$R = \frac{Q}{\Delta P} = \frac{8\mu l}{\pi r^4} \tag{17}$$

and

$$Q_k = \frac{\pi d_k^4}{128\mu} \frac{\Delta P_k}{l_k} \tag{18}$$

where ΔP_k and $d_k, l_k,$ represent the pressure drop, length, and hydraulic diameter of a branch at level k^{th}, respectively, and the channel and μ are the liquid viscosities, respectively. Based on equations (4)-(11) in terms of the ratio flow resistance radii and lengths of $\frac{R_{n-1}}{R_n}$ and $\frac{R_{n-2}}{R_{n-1}}$, the following relations are written.

$$\frac{R_{n-1}}{R_n} = \frac{r_n^4}{r_{n-1}^4} \times \frac{l_{n-1}}{l_n} \tag{19}$$

$$\frac{R_{n-2}}{R_{n-1}} = \frac{r_{n-1}^4}{r_{n-2}^4} \times \frac{l_{n-2}}{l_{n-1}} \tag{20}$$

As a result, the resistances in terms of the ratio of the resistances of the flow system in terms of α, β and γ are defined in relation to each other as follows.

$$\frac{R_{n-1}}{R_n} = \alpha^4 \beta^4 \gamma \tag{21}$$

$$\frac{R_{n-2}}{R_{n-1}} = \alpha^4 \beta^4 \gamma \tag{22}$$

The ratio of resistances between branches in terms of radii and lengths of $\frac{R_{n-1}}{R_n''}$ and $\frac{R_{n-2}}{R_{n-1}'}$ can be written as follows:

$$\frac{R_{n-1}}{R''_n} = \frac{r''^4_n}{r^4_{n-1}} \times \frac{l_{n-1}}{l''_n} \tag{23}$$

$$\frac{R_{n-2}}{R''_{n-1}} = \frac{r''^4_{n-1}}{r^4_{n-2}} \times \frac{l_{n-2}}{l''_{n-1}} \tag{24}$$

As a result, the resistances in terms of the ratio of the resistances of the flow system in terms of α, β, γ, λ, δ_1 and δ_2 are defined in relation to each other as follows:

$$\frac{R_{n-1}}{R''_n} = \alpha^4\gamma\delta_1\delta_2 \tag{25}$$

$$\frac{R_{n-2}}{R''_{n-1}} = \alpha^4\gamma\delta_1\delta_2 \tag{26}$$

Eqs. (18-21) were obtained by rearranging Eq. (1) by using the above relations. Based on series and parallel relationships, the flow resistance of the *N*th and (*N*-1)th branches is:

$$\begin{aligned} R_{n-1,total} &= R_{n-1}\left(1 + \frac{1}{\frac{1}{R_n} + \frac{1}{R'_n} + \frac{1}{R''_n}}\right) \\ &= R_{n-1}\left(1 + \frac{1}{\alpha^4\beta^4\gamma + \alpha^4\lambda^4\gamma\delta_1 + \alpha^4\gamma\delta_1\delta_2}\right) \end{aligned} \tag{27}$$

The flow resistance of the *N*th, (*N* - 1)th and (*N* - 2)th cycles is:

$$\begin{aligned} &R_{n-2,total} \\ &= R_{n-2} + \frac{1}{\frac{1}{R_{n-1,total}} + \frac{1}{R'_{n-1,total}} + \frac{1}{R''_{n-1,total}}} \\ &= R_{n-2}\left(1 + \frac{1}{\frac{R_{n-2}}{R_{n-1}} + \frac{R_{n-2}}{R'_{n-1}} + \frac{R_{n-2}}{R''_{n-1}}}\right) \\ &= R_{n-2}\left(1 + \frac{1}{\alpha^4\beta^4\gamma + \alpha^4\lambda^4\gamma\delta_1 + \alpha^4\gamma\delta_1\delta_2}\right. \\ &\left. + \left(\frac{1}{\alpha^4\beta^4\gamma + \alpha^4\lambda^4\gamma\delta_1 + \alpha^4\gamma\delta_1\delta_2}\right)^2\right) \end{aligned} \tag{28}$$

With the use of Eqs. (18) and (19) and mathematical relations:

$$\begin{aligned} &R_{n-t,total} \\ &= R_{n-t}\left(1 + \frac{1}{\alpha^4\beta^4\gamma + \alpha^4\lambda^4\gamma\delta_1 + \alpha^4\gamma\delta_1\delta_2}\right. \\ &+ \left(\frac{1}{\alpha^4\beta^4\gamma + \alpha^4\lambda^4\gamma\delta_1 + \alpha^4\gamma\delta_1\delta_2}\right)^2 + \cdots \\ &\left. + \left(\frac{1}{\alpha^4\beta^4\gamma + \alpha^4\lambda^4\gamma\delta_1 + \alpha^4\gamma\delta_1\delta_2}\right)^t\right) \end{aligned} \tag{29}$$

where $t < n$, and t =1, 2,3,. and $R_{n\text{-}t,total}$ is the total flow resistance from *N*th to the (*N* - *t*)th branch. Eq. (20) is a geometric progression. According to Eq. (20), let $t = n$, the total flow resistance of a two-level trifurcation network is written.

$$\begin{aligned} &R_{0,total} \\ &= R_0 \frac{1 - \left(\frac{1}{\alpha^4\beta^4\gamma + \alpha^4\lambda^4\gamma\delta_1 + \alpha^4\gamma\delta_1\delta_2}\right)^{n+1}}{1 - \frac{1}{\alpha^4\beta^4\gamma + \alpha^4\lambda^4\gamma\delta_1 + \alpha^4\gamma\delta_1\delta_2}} \end{aligned} \tag{30}$$

where R_0 is obtained via Eq. (21).

2.1.3. Trifurcation Structures in Flow Systems

Cases of two-level trifurcation flow systems with almost the same radii are discussed. When examining a two-level trifurcation flow system, due to the non-uniform features, some furcations may decrease at each progressive branch level, but their radius cannot reach zero or reach a minimum. Such structures are called trifurcation flow systems. As a result of the multiplication of the α and λ parameters (the ratio of the radii of the *n*"th and *n*-1th branches and the ratios of the radii of the *nth* and *n*"th branches), the following equation is obtained.

$$\frac{r_{n-1}}{r_n} = \left(\frac{1}{\alpha\lambda}\right) \tag{31}$$

The 0th and *n*th ratio of the radii of the two branches are given by the following equation, depending on α and λ.

$$\frac{r_0}{r_n} = \left(\frac{1}{\alpha\lambda}\right)^n \tag{32}$$

Given $\varepsilon = r_0/r_n$, n can be derived from Eq. (21) as follows:

$$\begin{aligned} \left(\frac{1}{\alpha\lambda}\right)^n = \varepsilon \quad &\rightarrow \quad n\ln\left(\frac{1}{\alpha\lambda}\right) = \ln\varepsilon \quad \rightarrow \quad n \\ &= -\frac{\ln\varepsilon}{\ln\left(\frac{1}{\alpha\lambda}\right)} \end{aligned} \tag{33}$$

From Eq. 20, the two-level trifurcation network is constructed according to $r_n = \alpha\lambda r_{n-1}$, $r'_n = \alpha\beta r_{n-1}$; if $\frac{r'_n}{r_0}$ is less than ε, the *n*th trifurcation is terminal (the extreme) trifurcation. For the trifurcation flow system from the terminal trifurcation to the 1st trifurcation shown in Fig. 1, the total flow resistance can be simply calculated by Eq. 30.

2.2. Computational Method

Recent studies have demonstrated CFD as an effective tool in optimizing fluid networks. Jia (2020) used CFD effectively to analyze fluid behavior in in high-speed traction motors. Ren et al. (2023) utilized it to investigate the motion characteristics of coarse particles in hydraulic collection systems. Ren (2024) studied the interaction of flow-transported materials with solid surfaces. Similarly, Bao et al. (2023) employed CFD in conjunction with deep learning to optimize the propulsive performance of flapping foils.

Based on the literature review on CFD applications in furcation flow systems, we employed CFD to analyze two alternative two-level trifurcation flow systems, while extending the application of Murray's Law to these configurations. To thoroughly analyze the flow behavior in trifurcation networks, CFD simulations were conducted using ANSYS Fluent. The governing equations for fluid motion, specifically the Navier-Stokes equations, were solved under the assumption of incompressible, steady-state, laminar flow. For all simulations, the working fluid was assumed to be water, as an incompressible fluid, with a constant density of 998.2 kg/m^3.

Table 2 Flow characteristics of branches of the trifurcation networks

Branch	Hydraulic Diameter (mm)	Velocity (m/s)	~Re
Main inlet	8.0	0.0800	400
First trifurcation	6.0	0.0504	190
Second trifurcation (side branches)	4.0	0.0390	100
Second trifurcation (middle branch in UD)	2.0	0.0400	150

To further validate the numerical approach, we report the Reynolds numbers (Re) at different branches of the trifurcation network. The Reynolds number is defined as:

$$Re = \frac{\rho U D}{\mu} \tag{34}$$

where ρ is fluid density, U is velocity, D is hydraulic diameter, and μ is dynamic viscosity. Based on the flow conditions, the Reynolds numbers for the primary inlet and individual branches are expected as detailed in Table 2.

These values confirm that the overall flow remains within the laminar regime (Re < 2000), supporting our choice of a laminar flow (White, 2006) model. However, prior research has demonstrated that flow separation and secondary vortices can occur even in laminar conditions due to geometric-induced instabilities. For instance, Guha and Pradhan (2017) investigated secondary flow structures in three-dimensional branching networks and found that even at moderate Reynolds numbers, local velocity gradients near furcations could introduce non-negligible shear effects. Similarly, Ostalowski and Tan (2022) performed direct simulations of blood flow in patient-specific microvascular bifurcations and observed that even for flows classified as laminar, small-scale turbulent fluctuations could arise due to junction-induced instabilities. Therefore, a secondary analysis was also conducted using the k-omega SST turbulence model in order to ensure robustness and account for potential local turbulence effects near junctions as well as to assess near-wall shear effects. The dimensionless wall distance parameter $y+$ was evaluated and kept below 5 to ensure that the boundary layer is adequately and accurately resolved, and the turbulence model does not introduce unnecessary numerical artifacts (Zhao et al., 2020).

This approach allows (1) ensuring that the computational model captures any local deviations from purely laminar behavior, and (2) validating whether turbulence-induced pressure losses or vortex formations significantly impact flow characteristics, such as alter flow resistance and pressure loss predictions. This methodology have been used in previous studies to resolve near-wall effects and secondary flow phenomena more accurately where complex geometries like trifurcation networks can exhibit localized turbulence effects even when the bulk flow is nominally laminar (Wilcox, 2006; Wang et al., 2018; Zhao et al., 2020).

The k-omega SST model is particularly well-suited for capturing shear layer effects in branching networks, as it provides a more refined treatment of near-wall regions compared to other models such as k-epsilon (Menter, 1994). On the other hand, Large Eddy Simulation (LES) is highly accurate for capturing transient turbulent structures but is computationally expensive for steady-state flow studies. Given the primarily laminar nature of the system, LES was deemed unnecessary.

2.3. Mesh Generation and Validation

Meshing is required before any CFD analysis. Mesh generation is a critical step to ensure accurate resolution of the flow field of a trifurcation model. For the accuracy of the results, the most suitable mesh structure must first be determined. Especially in the entrance sections close to the fractions, the mesh structure should be given in more detail for correct resolution. The computational domain was discretized using a tetrahedral mesh, with a total of 29,439,479 elements. To evaluate the mesh quality, metrics such as element skewness and orthogonality were monitored such that the final mesh ensures minimal numerical diffusion. Fig. 2 shows the final mesh produced by a quadratic equation at the endpoint of second level furcation. Meshing was applied to the whole model under the same conditions throughout the trifurcation flow system.

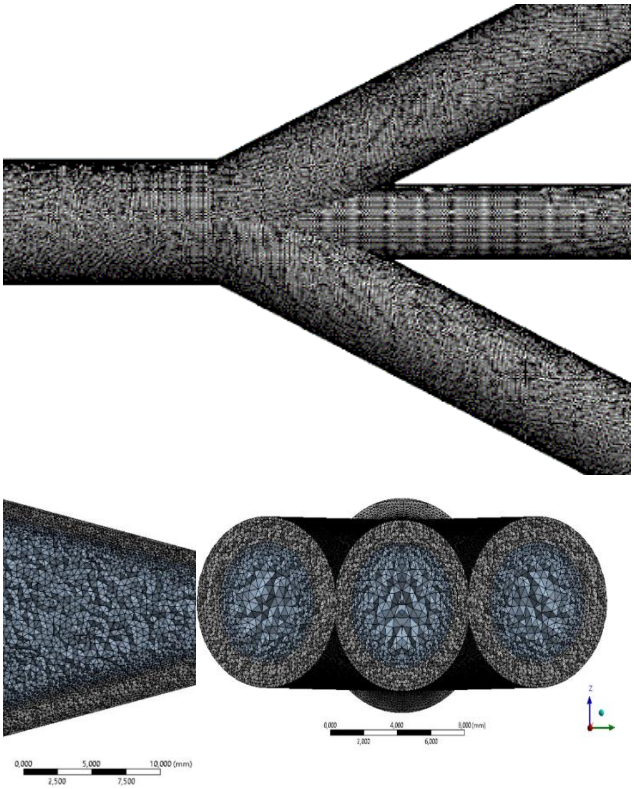

Fig. 2 A close-up views of generated mesh structure for CFD simulations

Table 3 Mesh quality and characteristics

Number of Nodes		11,458,347
Number of Elements		29,439,479
Skewness	Minimum	0.007
	Maximum	0.714
Orthogonality	Minimum	0.806
	Maximum	0.990
Aspect Ratio	Minimum	1.1186
	Average	1.6930
	Maximum	3.7560
Meshing Method		Patch Conforming (with tetrahedral elements)

The mesh used for the numerical simulations was created using the Patch Conforming method with tetrahedral elements to ensure high element quality and smooth transitions between flow regions. Instead of performing a formal grid independence study, we validated the accuracy of the mesh through quality metrics detailed in Table 3. As shown in Table 3, the mesh consisted of 11,458,347 nodes and 29,439,479 elements.

The mesh quality was confirmed by monitoring the skewness value. Skewness is a critical parameter in determining how well the elements are shaped and how accurately they represent the geometry. Skewness values below 0.9 are considered acceptable and values below 0.75 indicate good mesh quality. The skewness values of the generated mesh ranged from a minimum of 0.007 to a maximum of 0.714 and was well within acceptable limits for accurate CFD simulations (Ferziger & Perić, 2002).

While creating the solution mesh structure, the primary quality criterion considered for element quality was chosen the dimensionless wall distance parameter (y+). In the flow system, for the boundary layer between the liquid and the fluid on the inner surface of the flow pipe, the (y+) parameter is also examined by specifying the Wall Law region where the governing equations are solved due to the boundary layer, which is greatly affected by the fluid separation stress. In our case, for the selected mesh configuration of the designed trifurcation flow system, the minimum orthogonality was 0.806, and the y+ value is 4.7. Further, the mesh has an aspect ratio close to 1, ensuring uniform cell distribution without excessive stretching, which is evident from the finely-meshed model shown in Fig. 2.

The values of mesh quality metrics confirm that the chosen mesh provides accurate numerical results without requiring further refinement and tests. Since changes in flow parameters are dominated by physical conditions rather than numerical artifacts, additional grid refinement was deemed unnecessary.

Nevertheless, to ensure that numerical solution is independent of mesh refinement and accurately capture the flow physics without performing a full grid independence study, velocity gradients were evaluated across different regions of the computational domain, particularly in regions of high shear such as trifurcations, boundary layers, and recirculation zones.

In a poor mesh, the velocity gradients would exhibit excessive fluctuations or irregularities that do not align with physical expectations, which suggest that the grid is too coarse to resolve the flow structures adequately. Conversely, if velocity gradients are smooth and remain stable across successively refined meshes, it indicates that the numerical solution is grid-independent.

By evaluating velocity gradients given in in Fig. 6, Fig. 7 and Fig. 8, it can be ensured that the numerical diffusion introduced by discretization remains within acceptable limits and the key flow features, such as separation, recirculation, and boundary layer development, are all well-resolved since no artificial oscillations or unphysical behavior caused by under-resolution are identifiable.

By verifying the smoothness and consistency of velocity gradient distributions across the computational domain, we can gain confidence in the adequacy of the chosen mesh resolution without the need for excessive refinement studies.

2.3.1. Boundary Conditions and Solver Settings

The necessary boundary conditions for CFD simulations should be sufficient. The boundary conditions were carefully selected to replicate real-world scenarios. To evaluate the velocity in the trifurcation branched structures given in Fig. 5 and Fig. 6, the upstream inlet fluid velocity and atmospheric pressure are taken as boundary conditions. As the velocity boundary condition, the fluid uniform inlet velocity is taken as U_∞= 0.08 m/s, and for the wall boundary condition, at $r = 0$, the fluid velocity is $u = U_{max}$. No-slip boundary conditions were applied at $r=R$ as $u=0$ to account for viscous effects.

As the pressure boundary condition, the atmospheric pressure boundary condition at the inlet and the reference pressure at the branch outlets were used. These boundary conditions should be redefined at the beginning of the branching (junction) at each level so that they can be evaluated in detail. For this, experimental data of these points are needed. Then, more logical approaches can be developed. A detailed boundary condition information is presented in Table 4.

The simulations were performed in ANSYS Fluent using a pressure-based solver with a k-omega SST turbulence model to account for any turbulence effects in the flow. The initial simulations were conducted using the k-ω SST model, not because turbulence was expected, but rather as a verification strategy to ensure that no localized turbulence would affect the validity of a laminar flow assumption.

As per best practices in computational fluid dynamics (CFD), when the flow regime is uncertain or close to the laminar-turbulent transition, it is advisable to initially run turbulence models to identify any regions with potential flow instabilities or separation. In our case, the k-ω SST model served as a diagnostic tool to assess whether turbulent effects might arise in specific geometrical features or at higher local Reynolds numbers due to branching.

Table 4 Boundary conditions and solver settings

Boundary Type	Applied Condition	Description	Remarks
Inlet	Velocity Inlet: 0.08 m/s	Uniform velocity profile applied at the inlet.	Ensures controlled inflow conditions.
Outlet	Pressure Outlet: 0 Pa (Gauge)	Atmospheric pressure assumed at the outflow boundaries.	Prevents artificial backflow effects and allows natural outflow development
Walls	No-slip boundary condition	Zero velocity at solid walls.	Ensures adherence of fluid at the pipe walls, necessary for capturing boundary layer effects
Turbulence Model	k-omega SST	Used only for validation of local shear-layer effects near trifurcations.	Superior to k-epsilon for near-wall effects and flow separation
Wall Treatment	Low-Re Wall Functions with y+ < 5	Near-wall resolution ensures accurate boundary layer capture.	Essential for resolving shear stress distributions in trifurcations
Solver Scheme	Pressure-based solver	Steady-state incompressible Navier-Stokes equations solved.	Used in studies where compressibility is negligible
Discretization	Second-order upwind	Applied for momentum and turbulence equations.	Reduces numerical diffusion errors, ensuring accuracy in flow variables

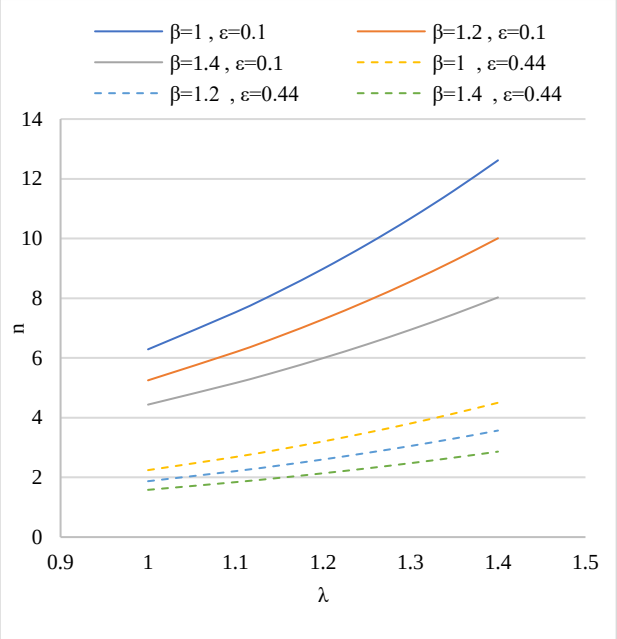

Fig. 3 Comparison of n against lambda for UD (solid) and ED (dashed) networks

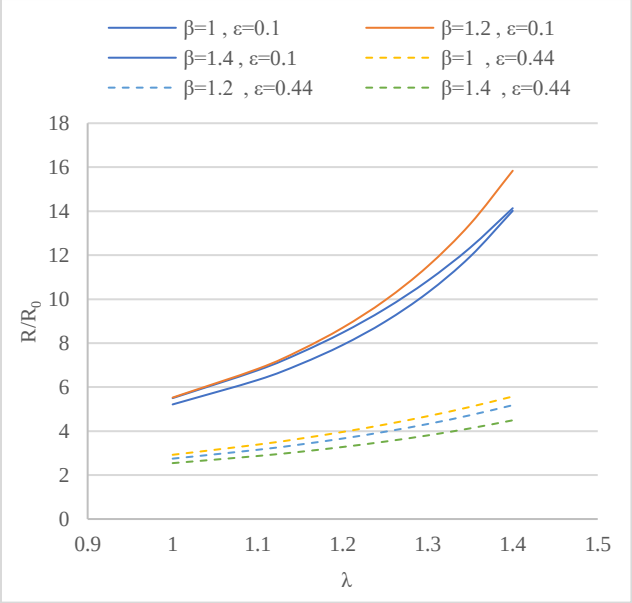

Fig. 4 Comparison R/R_0 against lambda for UD (solid) and ED (dashed) networks

The results from this preliminary step indicated that while some flow separation and minor recirculation zones could be detected—particularly near trifurcations or sharp curvature regions—these effects did not develop into sustained turbulence throughout the computational domain. Therefore, the flow regime was determined to remain predominantly laminar for the inlet velocity and Reynolds number range considered. Accordingly, all final simulations were performed using a laminar solver, which also simplified computation, avoided unnecessary turbulence modeling complexity, and aligned with the actual flow behavior in the model.

To improve the accuracy of the solutions, second-order upwind schemes were employed for momentum and pressure interpolation. The convergence criterion was set to a residual value of 10^{-5}.

3. RESULTS AND DISCUSSION

3.1. Analytic Results

With Eqs. (21) and (22), we can calculate the value of *n* for trifurcation with equal and different radii per stage, and the results are illustrated in Fig. 3 and Fig. 4 for the six conditions. The number of terminal trifurcations in ED trifurcation network is 3^n (n = 1, 2, 3). Therefore, for convenient comparison with the UD trifurcation networks,

Table 5 Comparison of geometrical parameters with a minimum radius

Parameters (β, λ, ε)	β=1, λ=1, ε=0.1	β=1, λ=1.25, ε=0.1	β=1.2, λ=1.25, ε=0.1	β=1, λ=1, ε=0.44	β=1, λ=1.25, ε=0.44	β=1.2, λ=1.25, ε=0.44
n	6.29	9.80	7.90	2.24	3.49	2.82
R/R_0	5.50	9.56	9.95	2.92	4.30	3.97

the number of terminal trifurcations in an UD trifurcation network must be 3^n. When ε=0.1 and β=1, the number of terminal trifurcation operations depends on λ, e.g., λ=1 is only 6, and for this number of terminal furcations, the resistance ratio is 5.5 for λ=1.4.

The terminal trifurcation number is 13, and for this number of terminal furcations, the resistance ratio is 14. For other values for β=1.2 and ε =0.1, we obtain the terminal trifurcation for λ=1 at approximately 6, the resistance ratio is 7, and for λ=1.4, it is 10, and the resistance ratio is 17. If we change the value of ε, for example, if ε is set to 0.44 for λ=1.25 and β=1.2, the terminal trifurcation will be 3, and the resistance ratio will be 3.97.

All these calculated values are shown in Table 5 and Table 6 as n and R/R_0 values calculated according to different values of λ, β and ε. We can determine the values of n and the resistance ratio for different values of λ, β and ε by using Eqs. 21 and 23, and then we can create the n and $\frac{R}{R_0}$ diagrams based on these geometrical parameters (λ, β and ε). Finally, we can construct the diagrams according to Fig. 3 and Fig. 4.

Fig. 3 and Fig. 4 show a comparison of flow resistance and branching behavior of the two trifurcation networks as described by the parameters λ, β, and ϵ. In Fig. 2, the relationship between n and λ show how different furcation configurations respond to changes.

Fig. 3 show that the increase in λ correspond to lesser flow resistance values in ED network. Notably in UD network, when β=1.2 and ϵ=0.1, the flow resistance rises sharply as λ exceeds 1.2, reaching up to 16 when λ=1.4. This sharp increase in resistance suggests that this specific configuration may become less efficient as the network branches further, leading to higher energy losses. In contrast, configurations with ϵ=0.44 show a much more gradual increase in flow resistance, staying below 8 even at the highest λ values, which is advantageous for efficient fluid transport.

A more comprehensive set of calculations for optimizing the trifurcation networks are presented in Table 6, which details the relationship between λ, β, and α that indicate how each branch in the network compares to its counterparts at different levels and the resulting flow resistance in combinations of these factors.

When ϵ=0.1, it is evident that the branching level n increases with as λ, accompanied by a proportional increase in R/R_0. This suggests that the network becomes more complex. For instance, in ED network when β=1.00 and λ=1.40, n reaches 12.62, with a corresponding R/R_0 value of 14.13 whereas in the UD network, n is 6.20 and flow resistance R/R_0 is 6.83 when β=1.20 and λ=1.10. As λ increases, both n and R/R_0 continue to rise, but the rate of increase in flow resistance appears to be more pronounced in UD networks compared to ED networks. This suggests that the introduction of variability in branch diameter leads to higher flow resistance.

When comparing the data across ϵ values, a lower ϵ resulting in higher values of n and R/R_0 can be said to be a reflection of denser network with greater resistance, vice versa. For instance, with β=1.40 and λ=1.4, the R/R_0 value for a UD network is 14.02 at ϵ=0.1, while it is significantly lower at 4.49 when ϵ=0.44, even though the network is still an UD type. The branching level k and ratios δ1, δ2, and γ provide additional understanding of the relation between geometric configurations of the network and flow characteristics.

The analysis shows that abrupt redirection of fluid results in localized flow separation and leads to higher energy dissipation and greater pressure losses, which are prominent in trifurcation networks with sharp branching transitions. For UD networks with a high λ value, the significant difference in branch diameters leads to velocity redistribution and can induce formation of recirculating vortices near the smaller branches.

3.1.1. Correlation Analysis

Previous studies (Zhao et al., 2020; Aghajannezhad & Sellier, 2022) have highlighted the importance of robust relational analyses in fluid systems. In this respect, a correlation analysis was performed to identify relationships between various parameters. Data obtained from theoretical calculations was analyzed to quantify the strength of relationships between parameters **ε**, λ, β, and n and their influences on the flow resistance, R/R_0. By employing correlation analysis, we aim to uncover the strength and direction of relationships among these variables. Table 7 presents the correlation matrix that indicates the relative strength of parameters that reflect different aspects of the system, such as network complexity and flow resistance, on each other on a scale -1 to 1, where -1 implies perfect negative relationship, 1 perfect positive relationship and 0 a linear relationship.

The correlation analysis reveals several key relationships between the variables. Firstly, there is a strong negative correlation between ε and n (-0.852), indicating that as ε increases, n tends to decrease. This suggests an inverse relationship between these two parameters, where changes in one are closely mirrored by opposite changes in the other. When analyzing R/R_0, it is strongly positively correlated with n (0.922), meaning that increases in n are accompanied by increases in R/R_0. Additionally, R/R_0 has a moderate positive correlation with λ (0.507), suggesting that λ also plays a role in influencing R/R_0, though to a lesser extent than n. In

Table 6 Calculation table of all geometrical parameters

ε	β	λ	n	α	δ1	δ2	γ	k	R/R_0	ED/UD
0.1	1.00	1.00	6.29	0.70	1.00	1.00	1.44	0.91	5.50	ED
0.1	1.00	1.10	7.53	0.67	1.00	1.10	1.49	0.94	6.76	ED
0.1	1.00	1.15	8.23	0.66	1.00	1.15	1.51	0.95	7.56	ED
0.1	1.00	1.20	8.98	0.65	1.00	1.20	1.54	0.96	8.48	ED
0.1	1.00	1.25	9.80	0.64	1.00	1.25	1.57	0.97	9.56	ED
0.1	1.00	1.30	10.67	0.62	1.00	1.30	1.61	0.99	10.84	ED
0.1	1.00	1.35	11.61	0.61	1.00	1.35	1.64	1.00	12.34	ED
0.1	1.00	1.40	12.62	0.60	1.00	1.40	1.67	1.01	14.13	ED
0.1	1.20	1.00	5.25	0.65	1.20	1.00	1.29	0.95	5.52	ED
0.1	1.20	1.10	6.20	0.63	1.20	1.10	1.32	0.98	6.83	UD
0.1	1.20	1.15	6.72	0.62	1.20	1.15	1.34	1.00	7.68	UD
0.1	1.20	1.20	7.29	0.61	1.20	1.20	1.36	1.01	8.70	UD
0.1	1.20	1.25	7.90	0.60	1.20	1.25	1.39	1.03	9.95	UD
0.1	1.20	1.30	8.56	0.59	1.20	1.30	1.41	1.04	11.50	UD
0.1	1.20	1.35	9.26	0.58	1.20	1.35	1.43	1.06	13.42	UD
0.1	1.20	1.40	10.01	0.57	1.20	1.40	1.46	1.07	15.84	UD
0.1	1.40	1.00	4.44	0.60	1.40	1.00	1.19	0.98	5.21	ED
0.1	1.40	1.10	5.16	0.59	1.40	1.10	1.22	1.01	6.32	UD
0.1	1.40	1.15	5.56	0.58	1.40	1.15	1.24	1.03	7.04	UD
0.1	1.40	1.20	5.99	0.57	1.40	1.20	1.25	1.04	7.91	UD
0.1	1.40	1.25	6.45	0.56	1.40	1.25	1.27	1.06	8.98	UD
0.1	1.40	1.30	6.94	0.56	1.40	1.30	1.29	1.07	10.29	UD
0.1	1.40	1.35	7.47	0.55	1.40	1.35	1.30	1.09	11.94	UD
0.1	1.40	1.40	8.03	0.54	1.40	1.40	1.32	1.11	14.02	UD
0.44	1.00	1.00	2.24	0.70	1.00	1.00	1.44	0.91	2.92	ED
0.44	1.00	1.10	2.68	0.67	1.00	1.10	1.49	0.94	3.38	ED
0.44	1.00	1.15	2.93	0.66	1.00	1.15	1.51	0.95	3.66	ED
0.44	1.00	1.20	3.20	0.65	1.00	1.20	1.54	0.96	3.96	ED
0.44	1.00	1.25	3.49	0.64	1.00	1.25	1.57	0.97	4.30	ED
0.44	1.00	1.30	3.81	0.62	1.00	1.30	1.61	0.99	4.68	ED
0.44	1.00	1.35	4.14	0.61	1.00	1.35	1.64	1.00	5.10	ED
0.44	1.00	1.40	4.50	0.60	1.00	1.40	1.67	1.01	5.57	ED
0.44	1.20	1.00	1.87	0.65	1.20	1.00	1.29	0.95	2.75	ED
0.44	1.20	1.10	2.21	0.63	1.20	1.10	1.32	0.98	3.15	UD
0.44	1.20	1.15	2.40	0.62	1.20	1.15	1.34	1.00	3.39	UD
0.44	1.20	1.20	2.60	0.61	1.20	1.20	1.36	1.01	3.66	UD
0.44	1.20	1.25	2.82	0.60	1.20	1.25	1.39	1.03	3.97	UD
0.44	1.20	1.30	3.05	0.59	1.20	1.30	1.41	1.04	4.32	UD
0.44	1.20	1.35	3.30	0.58	1.20	1.35	1.43	1.06	4.72	UD
0.44	1.20	1.40	3.57	0.57	1.20	1.40	1.46	1.07	5.18	UD
0.44	1.40	1.00	1.58	0.60	1.40	1.00	1.19	0.98	2.54	ED
0.44	1.40	1.10	1.84	0.59	1.40	1.10	1.22	1.01	2.87	UD
0.44	1.40	1.15	1.98	0.58	1.40	1.15	1.24	1.03	3.06	UD
0.44	1.40	1.20	2.14	0.57	1.40	1.20	1.25	1.04	3.28	UD
0.44	1.40	1.25	2.30	0.56	1.40	1.25	1.27	1.06	3.52	UD
0.44	1.40	1.30	2.48	0.56	1.40	1.30	1.29	1.07	3.80	UD
0.44	1.40	1.35	2.66	0.55	1.40	1.35	1.30	1.09	4.12	UD
0.44	1.40	1.40	2.86	0.54	1.40	1.40	1.32	1.11	4.49	UD

contrast, β shows a very weak correlation with R/R0 (-0.067), implying that it has little to no direct influence on this variable. However, β is highly correlated with other variables like γ (-0.898), δ1 (1.000), and k (0.675), indicating strong associations within this set of parameters, particularly between β, δ1, and γ.

The variable λ demonstrates moderate correlations with both R/R_0 (0.507) and k (0.726). This suggests that λ exerts some positive influence on these variables, indicating its role in the overall system dynamics, though its effect is not as pronounced as that of n on R/R0.

The analysis highlights that n is the most strongly correlated variable with R/R_0, while λ and k also show moderate relationships with both. Although β has strong relationships with other internal variables, it does not significantly influence R/R_0.

Table 7 Correlation matrix of system parameters with flow resistance

	ε	**β**	**λ**	**n**	**α**	**δ1**	**δ2**	**γ**	**k**	**R/R_0**
ε	1,000	0,000	0,000	-0,852	0,000	0,000	0,000	0,000	0,000	-0,789
β	0,000	1,000	0,000	-0,302	-0,768	1,000	0,000	-0,898	0,675	-0,067
λ	0,000	0,000	1,000	0,353	-0,626	0,000	1,000	0,411	0,726	0,507
n	-0,852	-0,302	0,353	1,000	0,001	-0,302	0,353	0,428	0,045	0,922
α	0,000	-0,768	-0,626	0,001	1,000	-0,768	-0,626	0,419	-0,966	-0,267
δ1	0,000	1,000	0,000	-0,302	-0,768	1,000	0,000	-0,898	0,675	-0,067
δ2	0,000	0,000	1,000	0,353	-0,626	0,000	1,000	0,411	0,726	0,507
γ	0,000	-0,898	0,411	0,428	0,419	-0,898	0,411	1,000	-0,325	0,266
k	0,000	0,675	0,726	0,045	-0,966	0,675	0,726	-0,325	1,000	0,328
R/R_0	-0,789	-0,067	0,507	0,922	-0,267	-0,067	0,507	0,266	0,328	1,000

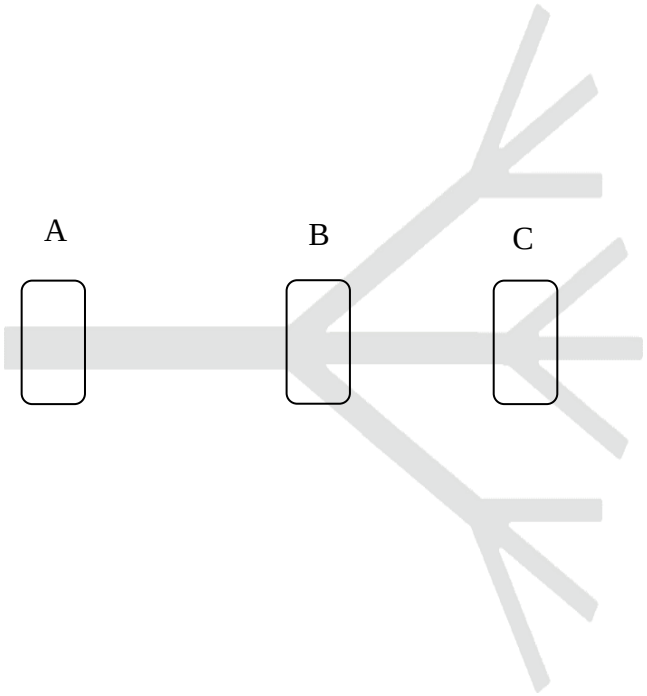

Fig. 5 Zones of fluid flow inspection illustrating velocity distribution

This can be explained by the fact that while β directly affects velocity redistribution and flow separation, its impact on overall resistance is dependent on R/R_0. In configurations where R/R_0 is close to 1 (ED networks), β has minimal influence on resistance. However, in UD networks, the relationship between branching angle and diameter variation creates complex secondary flow effects, which contribute to resistance in a non-linear manner. Furthermore, the strong correlation between β and energy dissipation highlights the role of branching geometry in determining shear-layer behavior and vortex formation. These findings suggest that branching geometry influence flow characteristics.

3.2. Numerical Results

The characteristics of the fluid flow through the trifurcation networks were evaluated comprehensively and discussed by analyzing velocity contours at various cross-sections of the network marked in Fig. 5. This figure shows the zones (A, B, and C) where various cross-sectional velocity profiles detailed in subsequent figures belong to.

In this section, one of the most important criteria in the tree-like ED and UD branched flow systems given in Fig. 6 and Fig. 7 is the analysis of velocity distributions at different levels and numbers of branches. Since the channels are generally symmetrical in such flow systems, it is ensured that the flow distribution is smooth in the relevant channel. The fluid flowing through the main inlet pipe divides into three groups at each branching point. The fluid flowing through three separate channels develops again until the next branching point. In the flow system, the analyses were performed under incompressible fluid and laminar flow conditions. Flow is simulated at each branch level and section to observe the flow patterns of the fluid passing through the trifurcation flow geometry shown in Fig. 5.

While the results are being examined during the solution process of the problem, for the ANSYS solutions, the numerical simulation results of the velocity distributions, especially around the furcation, are given for all three zones separately in Fig. 6, Fig. 7 and Fig. 8 for the 1st and 2nd branch levels at the x-y plane. Since velocity is a vector quantity, when the vector velocity distributions shown in Fig. 6 are examined, it is understood that the velocity values are different at the 1st and 2nd branch levels

In such flow systems, the simulated velocity vectors at the 1st and 2nd level furcation points and the eddy magnitude at low fluid velocity are shown. Likewise, while the velocity is maximal in the branch axes, it approaches zero toward the wall. In B and C zones, the flow is divided into three and new boundaries are formed on the inner walls of the ED and UD branches, respectively. Secondary flows and velocities occur due to flow separations in the furcation zone. The velocity of secondary flows occurring in the furcation zone is lower than the velocity of axial flows.

Velocity profiles across the trifurcation network exhibit significant gradients near furcation points, particularly in UD configurations. In ED networks, velocity remains uniformly distributed across branches, resulting in minimal pressure losses. However, in UD systems, the presence of higher velocity gradients leads to

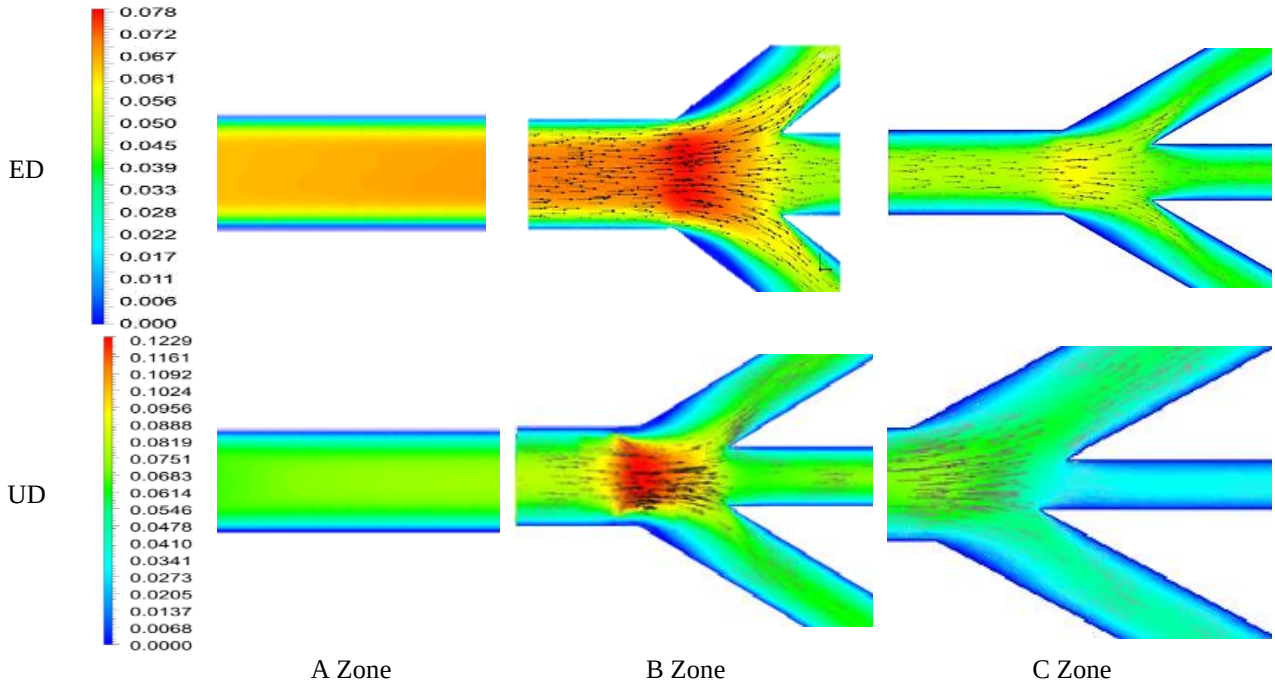

Fig. 6 Velocity profiles in the three inspection zones in the trifurcation fluid network

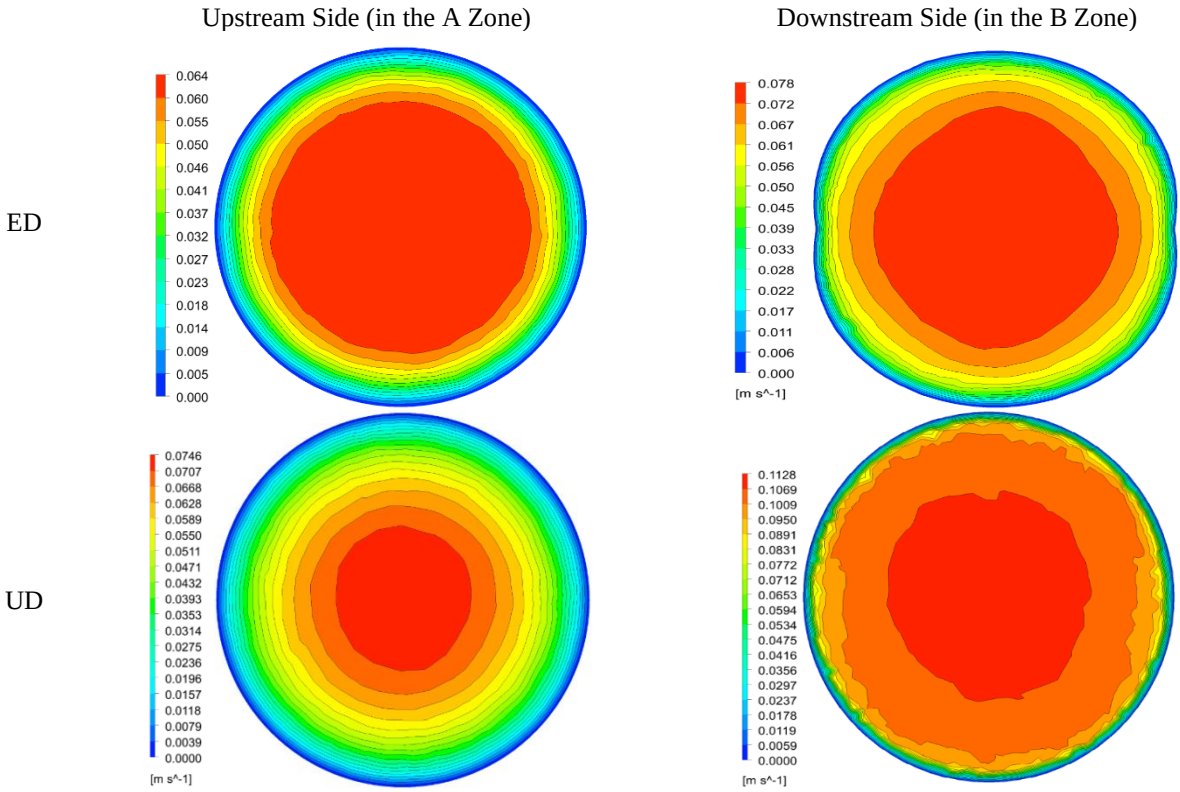

Fig. 7 Velocity profile in the main branch at the far side and near side of the furcation

increased shear stresses, which in turn amplify energy dissipation.

A direct relationship is observed between velocity gradients, pressure losses, and flow resistance, where:

$$\text{Energy Dissipation} \propto \frac{\partial u}{\partial x} \times \text{Viscous Shear Stress} \quad (35)$$

This suggests that regions with high velocity gradients experience more significant energy losses. In practical applications, such inefficiencies can be mitigated through gradual diameter transitions rather than abrupt variations in size and other geometrical parameters.

The velocity is very low where there are flow separations in the wall following the separation zone and in the regions close to the wall. The size of the furcation angle is important here. As the number of levels increases, the speed gradually decreases. Due to the structural design

features of fractal structures, the pipe diameter decreases at each level.

As shown in Fig. 6, cross-sections A-A, B-B, and C-C were taken separately on the flow system with two levels and three branches, and the fluid flow behavior in each branch section is shown. When the velocity profiles taken according to the cross sections are evaluated, it can be seen from the velocity profiles that the velocity values gradually decrease in successive similar cross sections.

For the ED network, in zone A, velocity distribution across the circular cross-section is relatively uniform, with the velocity highest in the center. The velocity gradually decreases toward the walls by forming concentric layers. This pattern is typical for laminar flow in a straight channel, where the fluid near the centerline moves faster due to reduced viscous drag compared to the fluid near the boundaries. The velocity in zone A reaches a maximum of approximately 0.064 m/s, indicating a stable and smooth flow before entering the furcation regions. The velocity distribution remains centered in zone B, but it shows a slight elongation along one axis, which indicates the beginning of the flow split as it encounters the furcation zone. As expected, the maximum velocity increases slightly to around 0.078 m/s as the flow accelerates to navigate through the narrowing channel.

In the 1st trifurcation, the flow has highly non-uniform velocity distribution and the velocity profile shows two distinct regions of high velocity surrounded by slower-moving fluid, which indicates that the flow is experiencing significant shear and acceleration at the furcation due to the convergence of streams from the parent branch into the daughter branches. The flow separation and reattachment in this zone contribute to the formation of vortices and complex flow patterns that are less stable than those observed in the previous zones.

In zone C, although contours are still slightly elliptical, velocity distribution shows a return to a more stable condition as the flow progresses through the trifurcation. The maximum velocity decreases to around 0.055 m/s, indicating that the flow has partially stabilized after the initial disturbances encountered in the 1st furcation in zone B. The overall pattern suggests that the flow is redistributing across the cross-section as it prepares to navigate further furcations or branch outs. Finally, in the second-level furcation, a velocity profile similar to that of the first-level furcation in zone B is evident with a more pronounced dumbbell-shaped distribution. The maximum velocity is slightly lower at approximately 0.049 m/s due to the energy losses incurred during the complex flow transitions and the continued redistribution of velocity within the trifurcation network. The symmetry observed in the velocity contours indicates that, the flow is moving towards a more uniform distribution as it progresses through the network.

For the UD network, shown in Fig. 6, the profiles are quite similar, but the impact of unequi-diameter furcation in the second-level, shown in zone C, can be seen to be influential all throughout the flow network. The highest velocity in zone A reaches approximately 0.0746 m/s, and around 0.1128 m/s zone B, followed by 0.0819 m/s in zone B and about 0.0697 m/sin zone C, all higher compared to the ED network. The maximum velocity in zone C, about 0.0659 m/s, is still around 25% higher compared the ED network.

It is clear that the flow undergoes significant changes in velocity and distribution as it navigates through the network. The highest velocities are observed near the initial trifurcation (zone B), where the flow accelerates into the narrower channels. The complexity of the flow reaches its peak at the 2nd trifurcation point (zone C), where the velocity profile exhibits the greatest degree of disturbance. This is likely attributable to the combined effects of flow splitting, acceleration, and local flow separation effects that result in transient velocity gradients. Although minor recirculation zones that are most suitable for the onset of turbulence were observed in the preliminary k-omega SST turbulence model simulations, no sustained turbulence developed across the domain and the flow remained predominantly laminar in the region under the investigated conditions. As the flow moves further downstream, it gradually stabilizes, with zone C showing a return to more organized and laminar flow patterns, though still influenced by the network's branching structure.

As a graphical representation of velocity plots given in Fig. 6, Fig. 7 and Fig. 8, the velocity distribution along the ED and UD networks are presented in Fig. 9.

As shown in Fig. 4 and Fig. 5, the forms of the average velocity of the liquid flow at different levels at different cross-sections are given for the inlet velocity of 0.08 m/s from the designed flow system. It can be seen from the graphs that the velocities in the flow center of the branches are greater than the velocities around the single and triple pipes.

To compare the results obtained from the CFD analysis against Murray's Law, we can see the drawbacks the analytical approach has. First of all, Murray's law assumes equal or directly proportional division of flow among all daughter branches, as given in Eq. (2), but numerical results show that it does not hold in the case of unequal diameter branching. As can be seen in Fig. 6, the center daughter in the second level has a remarkably lower velocity profile in the UD network than in the ED network, as a result that unequal branching disrupts mass conservation assumptions and leads to higher localized resistance in the smaller diameter branch. It is also noticeable in Fig. 7 that velocity gradients are asymmetric in the C zone in UD network. This can be attributed to the fact that additional energy dissipation, which is a phenomenon not accounted by Murray's Law, occurred and localized turbulent effects may have developed and increased effective flow resistance beyond what was predicted by the equations. This suggests that flow resistance is not evenly distributed among daughters as well.

The CFD results for the system were validated against the analytical solutions. An error percentage was calculated using the formula:

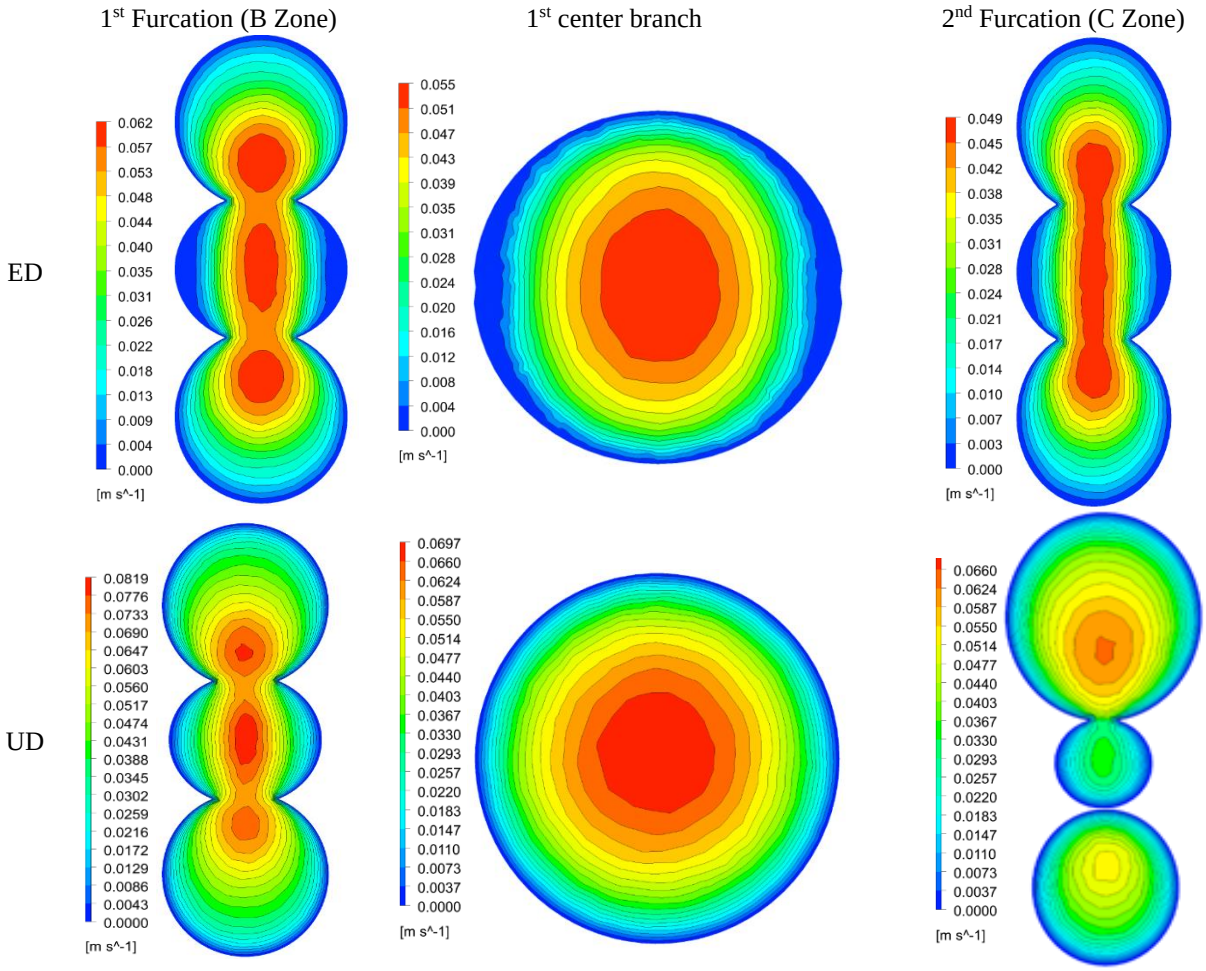

Fig. 8 Velocity distribution in the first furcation zone and center branches

$$\text{Error\%} = \left(\frac{|\ \text{Analytical} - \text{Numerical}\ |}{\text{Analytical}}\right) \times 100 \quad (36)$$

The relative error between the CFD results and the analytical predictions for flow velocity was consistently below 5% for the ED network. For the UD network, however, the error percentages are almost always around 15%. This suggests that the Murray's law has serious drawbacks in asymmetric or non-uniform network configurations.

3.3. Comparison of the Two Trifurcation Networks

In both networks, the flow in zone A shows a relatively constant and laminar distribution. But the maximum velocity was approximately 0.064 m/s in the ED network and 0.0746 m/s in the UD network. When the flow moves towards the zone B, the differences between the networks become apparent. In the ED network, the maximum velocity increases to about 0.078 m/s, and the velocity distribution extends along one axis due to the approaching furcation. In contrast, there is a more pronounced acceleration in the UD network, with the maximum velocity reaching 0.1128 m/s, and the asymmetry in the velocity profile becomes more pronounced. This suggests that the UD network has a more sudden transition at the furcation point, which can result in higher flow rates and increased shear forces.

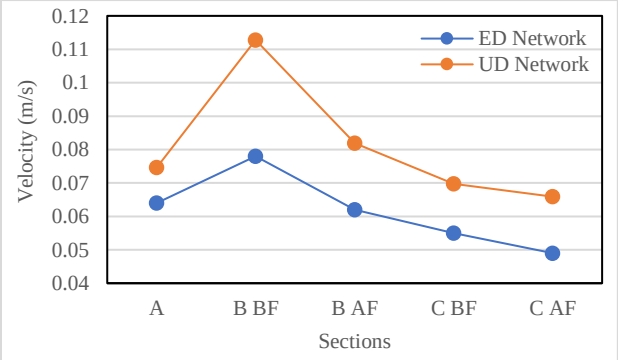

Fig. 9. Comparison of maximum velocity at cross-sections in two flow networks

In B zone, in both networks the most complex flow behaviors were observed. At the 1st furcation in zone B, both networks revert to a more symmetrical and circular velocity distribution, while the maximum velocity in the UD network (0.0697 m/s) is slightly higher than in the ED network (0.055 m/s). These findings reveal that both networks allowed the flow to stabilize after the initial furcation, but the UD network showed a slower recovery due to higher speeds and complex flow patterns. In the ED, the maximum velocity was approximately 0.062 m/s whereas in UD velocity is higher at 0.0819 m/s. The more

pronounced velocity gradients and complex flow patterns in the UD network clearly indicate a higher degree of disruption to the flow due to the narrower center-branch diameter. As the flow progresses towards the second-level furcation point, it appears that the velocity profiles on both networks begins to stabilize. In the 2nd furcation in zone C, the velocity in the ED network (0.049 m/s) was lower than in the UD network (0.0659 m/s), indicating lower energy dissipate.

In terms of velocity distribution and energy dissipation, the UD network is more prone to energy losses and turbulence formation than the ED network with higher maximum speeds and more complex flow patterns. In both the ED and UD network, the flow distribution stabilized after the first furcation, but the recovery in the UD network was slower, indicating that the narrower diameter in the middle channel increased the furcation effect and increased energy losses. Therefore, it becomes clear that channel diameters should be carefully evaluated in the optimization of trifurcation networks. CFD simulations show distinct differences in flow behavior between ED and UD trifurcation networks. In the ED network, the flow is distributed more evenly across the branches, resulting in lower vorticity and reduced flow separation at branching points. This supports the predictions of Murray's Law, which suggests that flow resistance is minimized when branch diameters are balanced.

From a fluid dynamics standpoint, the higher flow resistance in the UD network suggests that careful attention must be given to the geometric design of trifurcation systems to optimize flow efficiency. Our results underscore the importance of balancing branch diameters to maintain smooth flow transitions and minimize pressure losses.

4. CONCLUSION

This study confirmed that Murray's law can be effectively applied in optimization of flow distribution in trifurcation flow networks. Using computational fluid dynamics (CFD) simulations, we evaluated both equi-diameter (ED) and unequal-diameter (UD) trifurcation networks to analyze flow resistance, velocity distribution, and energy losses. The results confirmed that the losses in the trifurcation flow systems are directly linked to the geometrical properties of the network, with a strong correlation between vortex formation and energy dissipation. Additionally, analyses were performed to determine a more effective flow profile around the branch departure point.

Changes in the angle, level, furcation number and fluid flow rate significantly affect the flow resistance and pressure of the system. In a fractal-like trifurcation flow system, the inlet and outlet of the flowing fluid and the resistance can significantly reduce the pressure drop between the inlet and outlet of the system. Analytical solutions become more complex as the level of branching and the number of furcations increase. Therefore, to provide the appropriate flow profile formed at the furcation zones, analyses of the flowing fluid are performed in ANSYS.

In the ED network, flow resistance was minimized, and vorticity remained low due to more uniform flow distribution across the branches. This finding is consistent with the predictions of Murray's Law, which posits that equal branch diameters lead to optimized flow efficiency. The UD network exhibited higher velocities in the narrower branches, which resulted in greater shear forces, flow separation, and the formation of localized vortices. Increased pressure drops and energy losses were observed, particularly in the first and second-level furcation. Velocity profiles across the ED network were smoother and more symmetric compared to the UD network, which exhibited sharper velocity gradients and more turbulence, highlighting the inefficiencies introduced by unequal diameters.

According to the results obtained in this study, it is thought that trifurcation microflow systems with such branched properties will be very important in engineering applications in terms of future designs. Specifically, designing systems with more balanced branch diameters, as in ED networks, can minimize pressure drops and enhance flow efficiency. On the other hand, careful consideration must be given to the design of UD systems, which, although potentially more flexible, can lead to increased energy loss. The implications can practical in lab-on-chip systems in improvement of fluidic channel designs for controlled sample distribution and reagent mixing, as well as optimizing droplet generation and flow partitioning. Cooling systems and heat exchangers are another application field that can draw conclusions from the finding of this study in improving coolant distribution efficiency and in minimizing pumping power losses.

Future research could extend these findings by using different and more complex designs, incorporating diverse fluid properties, introducing varying viscosities and densities in the simulation models. Using more sophisticated optimization algorithms, particularly for complex geometries and non-linear fluid behaviors, will add further insight into enhancing the efficiency of trifurcation networks. Moreover, non-uniform, asymmetric and complex trifurcation systems require further investigation and exploration, machine learning or genetic algorithms can be used to optimize trifurcation network designs for minimal energy dissipation. Future research can also address high Reynolds numbers and advanced turbulence modelling such as Large Eddy Simulation (LES) or Direct Numerical Simulation (DNS) to capture turbulence-induced flow instabilities near trifurcation points.

5. LIMITATIONS

The present study relies solely on analytical and numerical simulation. While CFD is a powerful tool for analyzing fluid flow, it can be sensitive to boundary conditions and turbulence models. Therefore, experimental studies are necessary to validate these findings. Additionally, Murray's law does not account for dynamic fluid properties, such as viscosity and density. Future research could benefit from integrating these factors into the optimization framework in order to accurately reflect fluid behavior under diverse conditions.

CONFLICT OF INTEREST

The authors declare that there is no conflict of interest.

AUTHORS CONTRIBUTION

M. Mustafaoğlu: Conceptualization, Methodology, Modeling; Software, Data analysis; Writing-initial draft. **M. Kaan Yeşilyurt:** Investigation, Modeling, Resources, Data curation; Writing-initial draft, Writing-review & editing. **İ. Kotcioglu:** Supervision; Writing-review & editing. **M. Allahyari:** Investigation, Writing- initial draft.

REFERENCES

Aghajannezhad, P., & Sellier, M. (2022). The effects of surface roughness on the flow in multiple connected fractures. *Fluid Dynamics Research. 54*(1), Article 015504. https://doi.org/10.1088/1873-7005/ac49a1

Balogh, P., & Bagchi, P. (2018). Analysis of red blood cell partitioning at bifurcations in simulated microvascular networks. *Physics of Fluids*, *30*(5), Article 051902. https://doi.org/10.1063/1.5024783

Bao, Y. Shi, X., Wang, Z [Zhipeng], Zhu, H., Srinil, N., Li, A., Zhou, D., & Fan, D. (2023). Deep reinforcement learning for propulsive performance of a flapping foil. *Physics of Fluids*, *35*(10), Article 103610. https://doi.org/10.1063/5.0169982

Beighley, R., Spedden, E., Sekeroglu, K., Atherton, T. J., Demirel, M. C., & Staii, C. (2012). Neuronal alignment on asymmetric textured surfaces. *Applied Physics Letters*, *101*(14), Article 143701. https://doi.org/10.1063/1.4755837

Bejan, A. (1997). Constructal tree network for fluid flow between a finite-size volume and one source or sink. *Revue Generale De Thermique*, *36*(8), 592-604. https://doi.org/10.1016/S0035-3159(97)89986-2

Bejan, A. (2000). *Shape and structure, from engineering to nature*. Cambridge university press. ISBN: 0521793882

Bejan, A. (2001). The tree of convective heat streams: its thermal insulation function and the predicted ¾-power relation between body heat loss and body size. *International Journal of Heat and Mass Transfer*, *44*(4), 699–704. https://doi.org/10.1016/S0017-9310(00)00138-1

Bejan, A., & Errera, M. R. (1997). Deterministic tree networks for fluid flow: geometry for minimal flow resistance between a volume and one point. *Fractals*, *5*(04), 685–695. https://doi.org/10.1016/S0035-3159(97)89986-2

Calamas, D., & Baker, J. (2013). Tree-like branching fins: Performance and natural convective heat transfer behavior. *International Journal of Heat and Mass Transfer*, *62*, 350–361. https://doi.org/10.2514/1.T3950

Chen, Y. (2024). Flow and heat transfer performance of asymmetric fractal tree network in fractal porous media. *Physics of Fluids*, *36*, Article 023319. https://doi.org/10.1063/5.0193677

Chen, Y. [Yongping], & Cheng, P. (2002). Heat transfer and pressure drop in fractal tree-like microchannel nets. *International Journal of Heat and Mass Transfer*, *45*(13), 2643-2648. https://doi.org/10.1016/S0017-9310(02)00013-3

Doyeux, V., Podgorski, T., Peponas, S., Ismaïl, M., & Coupier, G. (2011). Spheres in the vicinity of a bifurcation: elucidating the zweifach–fung effect. *Journal of Fluid Mechanics*, *674*, 359-388. https://doi.org/10.1017/s0022112010006567

Ferziger, J. H., & Perić, M. & Street, R. L. (2020). Computational Methods for Fluid Dynamics (3rd, rev. ed.). Springer International Publishing. https://doi.org/10.1007/978-3-319-99693-6

Guha, A., & Pradhan, K. (2017). Secondary motion in three-dimensional branching networks. *Physics of Fluids*, *29*(6), Article 063602. https://doi.org/10.1063/1.4984919

Guha, A., & Sengupta, S. (2016). Effects of finiteness on the thermo-fluid-dynamics of natural convection above horizontal plates. *Physics of Fluids*, *28*(6), Article 063603. https://doi.org/10.1063/1.4953382

Jia, J. (2020). Analysis of temperature rise in high-speed permanent magnet synchronous traction motors by coupling the equivalent thermal circuit method and computational fluid dynamics. *Fluid Dynamics & Materials Processing*, *16*(5), 919-933. https://doi.org/10.32604/fdmp.2020.09566

Kawano, T., & Fuchiwaki, M. (2022). Pressure drop mechanisms in a cooling system enclosure. *Journal of Fluid Science and Technology*, *17*(4), Article JFST0014. https://doi.org/10.1299/jfst.2022jfst0014

Kim, Y., & Peskin, C. S. (2008). Numerical study of incompressible fluid dynamics with nonuniform density by the immersed boundary method. *Physics of Fluids*, *20*(6), Article 062101. https://doi.org/10.1063/1.2931521

Luo, L., Tian, F., Cai, J., & Hu, X. (2018). The convective heat transfer of branched structure. *International Journal of Heat and Mass Transfer*, *116*, 813-816. https://doi.org/10.1016/j.ijheatmasstransfer.2017.09.056

Menon, K. (2024). Cardiovascular fluid dynamics: a journey through our circulation. *Flow*, *4*, Article E7. https://doi.org/10.1017/flo.2024.5

Menter, F. R. (1994). Two-equation eddy-viscosity turbulence models for engineering applications. *AIAA Journal*, *32*(8), 1598–1605. https://doi.org/10.2514/3.12149

Murray, C. D. (1926a). The physiological principle of minimum work applied to the angle of branching of arteries. *The Journal of General Physiology*, *9*(6), 835.

Murray, C. D. (1926b). The physiological principle of minimum work. I: The vascular system and the cost of blood volume. *Proceedings of the National Academy of Sciences of the United States of America*, *12*(5), 207-214. http://www.jstor.org/stable/85001

Murray, C. D. (1927). A relationship between circumference and weight in trees and its bearing on branching angles. *The Journal of General Physiology*, *10*(5), 725- 729. https://doi.org/10.1085/jgp.10.5.725

Ostalowski, K., & Tan, J. (2022). Direct simulation of blood flow with heterogeneous cell suspensions in a patient-specific capillary network. *Physics of Fluids*, *34*(4), Article 041912. https://doi.org/10.1063/5.0088342

Pradhan, K., & Guha, A. (2019). Fluid dynamics of oscillatory flow in three-dimensional branching networks. *Physics of Fluids*, *31*(6), Article 063601. https://doi.org/10.1063/1.5093724

Ren, W., Zhang, X., Zhang, Y., & Lu, X. (2023). Investigation of motion characteristics of coarse particles in hydraulic collection. *Physics of Fluids*. *35*(4), Article 043322. https://doi.org/10.1063/5.0142221

Ren, Y. (2024). Coupled CFD-DEM numerical simulation of the interaction of a flow-transported rag with a solid cylinder. *Fluid Dynamics & Materials Processing*, *20*(7), 1593-1609. https://doi.org/10.32604/fdmp.2024.046274

Smink, J. S., Venner, C. H., Visser, C. W., & Hagmeijer, R. (2023). Engineering of branched fluidic networks that minimise energy dissipation. *Journal of Fluid Mechanics*, *967*(A6). https://doi.org/10.1017/jfm.2023.433

Wang, Z., Sui, Y., Salsac, A. V., Barthès-Biesel, D., & Wang, W. (2018). Path selection of a spherical capsule in a microfluidic branched channel: towards the design of an enrichment device. *Journal of Fluid Mechanics*, *849*, 136-162. https://doi.org/10.1017/jfm.2018.414

White, F. M. (2006). *Viscous Fluid Flow* (3rd ed.). McGraw Hill. ISBN: 978-0072402315.

Wilcox, D. C. (2006). *Turbulence modeling for CFD* (3rd ed.). DCW Industries. ISBN: 9781928729082

Xu, P., & Yu, B. (2006). The scaling laws of transport properties for fractal-like tree networks. *Journal of Applied Physics*, *100*(10), Article 104906. https://doi.org/10.1063/1.2392935

Ye, T., & Peng, L. (2019). Motion, deformation, and aggregation of multiple red blood cells in three-dimensional microvessel bifurcations. *Physics of Fluids*, *31*(2), Article 021903. https://doi.org/10.1063/1.5079836

Yu, X., Zhang, C., Teng, J., Huang, S., Jin, S., Lian, Y., Cheng, C., Xu, T., Chu, J. -C., & Chang, Y. -J. (2012). A study on the hydraulic and thermal characteristics in fractal tree-like microchannels by numerical and experimental methods. *International Journal of Heat and Mass Transfer*, *55*(25-26), 7499–7507. https://doi.org/10.1016/j.ijheatmasstransfer.2012.07.050

Zhao, B., Wang, Z., Duan, W., Ertekin, R. C., Hayatdavoodi, M., & Zhang, T. (2020). Experimental and numerical studies on internal solitary waves with a free surface. *Journal of Fluid Mechanics*, *899*, Article A17. https://doi.org/10.1017/jfm.2020.451

Zimmerman, R. A., & Tartakovsky, D. M. (2020). Solute dispersion in bifurcating networks. *Journal of Fluid Mechanics*, *901*, Article A24. https://doi.org/10.1017/jfm.2020.573